

## Central Lancashire Online Knowledge (CLoK)

Title	Assessing wire EDM as a novel approach for CFRP drilling: performance and thermal analysis across lay-up configurations
Type	Article
URL	<a href="https://clock.uclan.ac.uk/52434/">https://clock.uclan.ac.uk/52434/</a>
DOI	##doi##
Date	2024
Citation	Bajoria, Aman, Al Shaer, Ahmad Wael orcid iconORCID: 0000-0002-5031-8493 and Abdallah, Ramy (2024) Assessing wire EDM as a novel approach for CFRP drilling: performance and thermal analysis across lay-up configurations. International Journal of Advanced Manufacturing Technology . ISSN 0268-3768
Creators	Bajoria, Aman, Al Shaer, Ahmad Wael and Abdallah, Ramy

It is advisable to refer to the publisher's version if you intend to cite from the work. ##doi##

For information about Research at UCLan please go to <http://www.uclan.ac.uk/research/>

All outputs in CLoK are protected by Intellectual Property Rights law, including Copyright law. Copyright, IPR and Moral Rights for the works on this site are retained by the individual authors and/or other copyright owners. Terms and conditions for use of this material are defined in the <http://clock.uclan.ac.uk/policies/>



# Assessing wire EDM as a novel approach for CFRP drilling: performance and thermal analysis across lay-up configurations

Aman Bajoria<sup>1</sup> · Ahmad Alshaer<sup>2</sup> · Ramy Abdallah<sup>1,3</sup>

Received: 8 February 2024 / Accepted: 18 July 2024  
© The Author(s) 2024

## Abstract

Conventional drilling of carbon fibre–reinforced plastic (CFRP) presents significant challenges due to the material’s abrasive nature and anisotropic properties, leading to tool wear, delamination, and surface damage. To address these challenges, this study pioneers the use of wire electrical discharge machining (WEDM) to evaluate the drilling performance of thick CFRP lay-up configurations mainly unidirectional and multidirectional, marking the first application of WEDM for CFRP drilling. The study evaluates material removal rate (MRR), delamination factor (DF), and surface damage while employing an analytical solution to estimate surface temperature and heat conduction in the laminates. An eight-full factorial experimental design was employed, involving variations in ignition current (3 A and 5 A) and pulse-off time (4  $\mu$ s and 8  $\mu$ s). The findings revealed that the multidirectional lay-up achieved an MRR of 2.85 mm<sup>3</sup>/min, significantly outperforming the unidirectional lay-up’s MRR of 0.95 mm<sup>3</sup>/min, representing a 300% increase at 5 A and 4  $\mu$ s. However, the increase in discharge energy led to surface damage such as delamination, frayed fibres, and irregular circularity, especially evident in the unidirectional lay-up. For delamination, the multidirectional lay-up had the highest top DF of 1.4 at 5 A and 6  $\mu$ s, while the unidirectional lay-up achieved the peak bottom DF of 1.24 at the same levels. While none of the parameters significantly affected the responses, the current exhibited the highest contribution ratios. Analytical predictions of the thermal distribution indicated a 45- $\mu$ m delamination length at the laminate surface and depth, aligning closely with experimental predictions of 30–50  $\mu$ m.

**Keywords** Electrical discharge machining · Material removal rate · Delamination · Thermal modelling · Carbon fibre–reinforced plastic

## 1 Introduction

Carbon fibre–reinforced plastic (CFRP) is a composite material consisting of a resin matrix (e.g. epoxy) reinforced with carbon fibres [1]. It is valued for its lightweight nature (with a density ranging from 1.5 to 2 g/cm<sup>3</sup>), high specific stiffness (approximately 75–105% of steel), and impressive strength

(approximately 785 kN·m/kg) [2]. CFRPs demonstrate notable fatigue and corrosion resistance [3], exceptional damping characteristics, elevated rigidity, as well as minimal dimensional changes during heating [4]. Over the past 50 years, these features have significantly driven the adoption of CFRP in both aerospace and non-aerospace industries, including automotive, transportation, and energy sectors, with an annual growth rate of 12.5% over the last two decades [5, 6]. However, the COVID-19 pandemic significantly reduced global CFRP demand, resulting in a 30% decline in aerospace market consumption. The low cost of carbon fibre production is expected to drive future demand, with estimates reaching up to 200 kt for wind turbines, 180 kt for pressure vessels, and 100 kt for automotive and rail transportation by 2030. Recent aircraft such as the Airbus A350 and Boeing 787 incorporate CFRP for more than 50% of their weight, contributing to substantial fuel savings and lower exhaust emissions [6, 7]. The extensive use of CFRP in the aircraft industry underscores the critical role of drilling as a

✉ Ramy Abdallah  
r.m.a.m.abdallah@bham.ac.uk;  
ramy\_abdulnabi@h-eng.helwan.edu.eg

<sup>1</sup> Machining Research Group, Department of Mechanical Engineering, School of Engineering, University of Birmingham, Edgbaston, Birmingham, UK

<sup>2</sup> Advanced Manufacturing Group, School of Engineering and Computing, University of Central Lancashire, Preston, UK

<sup>3</sup> Production Engineering Department, Faculty of Engineering, Helwan University, Helwan, Cairo, Egypt

pivotal machining process. This process is particularly crucial for creating bolt or rivet holes during aircraft assembly, with large cargo planes requiring up to 1 million such holes. The quality of these holes significantly affects the service life of the aircraft [5, 8]. However, the abrasive nature, heterogeneity, and anisotropic behaviour of carbon fibres result in pronounced tool wear and give rise to surface imperfections, including frayed fibres, delamination, matrix fractures, splintering, and burrs [9–12]. Consequently, research has increasingly focused on alternative machining processes to mitigate the surface damage often encountered during conventional methods. Exploration of non-conventional machining methods, including abrasive waterjet, ultrasonic, and laser beam machining, provides benefits such as decreased tool wear, minimized delamination, and reduced cutting force requirements [13–15]. However, these techniques are not flawless, as they can lead to specific failure modes during cutting, such as “steplike delamination, interlaminar cracks, and high-density micro-failure zones” [16], along with heat-affected zones (HAZ) [17]. Electrical discharge machining (EDM) is another non-conventional process being explored for CFRP. However, the inherent low conductivity of CFRP, due to its resistive resin matrix [18], represents a significant hindrance to the effectiveness of EDM. As a result, research on EDM of CFRP has been relatively limited compared to other techniques.

Among the earliest investigations into the utilization of die-sink EDM for CFRP, Lau et al. [19] conducted a thorough investigation into key machining parameters such as peak current, pulse duration, tool material, and tool polarity. They found that peak current directly influenced material removal rate (MRR), peaking at approximately  $10.5 \text{ mm}^3/\text{min}$  with 1 A, but declining at higher currents due to excessive heat. Tool wear rate initially decreased up to 1 A peak current before increasing significantly. Surface roughness ranged from  $15 \text{ }\mu\text{m}$  at 1 A to  $45 \text{ }\mu\text{m}$  at 4 A. Pulse-on and pulse-off times were critical, with longer pulse-on times increasing MRR, and adjusting pulse-off times up to 300  $\mu\text{s}$  enhanced MRR for copper and graphite electrodes. The study underscored the influence of these parameters on MRR, wear characteristics, and the microscopic heterogeneity caused by thermal effects at high currents, impacting resin bonding among fibres in the EDMed surface. Similarly, the impact of cutting directions (parallel and perpendicular to fibre orientation) on various response metrics was assessed for different CFRP structures, primarily unidirectional and bidirectional [20, 21], and compared against SKD11. The results showed that CFRP demonstrated superior machinability with EDM, achieving higher MRRs ( $\sim 5 \text{ mm}^3/\text{min}$ ) across different workpiece structures and cutting directions compared to SKD11 ( $0.2 \text{ mm}^3/\text{min}$ ) at low current. Furthermore, Sheikh-Ahmed and Shinde [8] studied how electrode type affects CFRP drilling performance under

varied conditions. Graphite electrodes showed superior MRR, and lower wear rates compared to copper electrodes across different currents. Likewise, Habib and Okada [16] found graphite electrodes consistently achieved higher MRR than copper electrodes. They optimized surface roughness by adjusting pulse-off time and rotational speed, achieving a minimum gap size of 1.8 mm at 1000 rpm. Wear rate decreased with higher current, pulse-on time, and voltage, reaching minimal levels at 2.5 A, 100  $\mu\text{s}$ , and 120 V. Likewise, Roldan-Jimenez et al. [22] found that using higher capacitance values in a radiofrequency (RF) relaxation circuit during the drilling of unidirectional CFRP improved material removal rates (MRR) and produced larger holes. However, this technique compromised surface quality, resulting in higher surface roughness (Ra) values and greater thermal damage at the edges. On the other hand, the impact of using an aluminium fixture while drilling 1-mm-thick CFRP on hole quality attributes, such as tool wear, material removal rates, hole circularity/taper, and entrance/exit diameter, was evaluated [23]. Grey relational analysis (GRA) and an artificial neural network (ANN) optimized and correlated machining parameters (peak current, pulse on/off time, and flushing pressure) with responses. Pulse-on time had the most significant influence, followed by current, pulse-off time, and flushing pressure. Under optimal conditions (4 A, 25- $\mu\text{s}$  pulse on/off time, 0.6 MPa flushing pressure), results showed a low taper angle ( $-0.81354^\circ$ ), minimal tool wear ( $0.000069 \text{ g/min}$ ), uniform circularity (0.979), and negligible burr formation with  $350.7\text{-}\mu\text{m}$  delamination, compared to an initial burr length of  $391.75 \text{ }\mu\text{m}$  and  $539.3\text{-}\mu\text{m}$  delamination. Recently, Chen et al. [24] explored the utilization of a graphene aqueous solution as a dielectric in EDM of CFRP (1.5 mm thick), comparing it with kerosene and deionized water. The study aimed to evaluate the impact on MRR, EWR, and HAZ. Results showed a 76% higher MRR with graphene compared to kerosene and an 18% improvement over deionized water. The inclusion of graphene nanoparticles expanded the discharge gap, enhancing overall removal efficiency. Scanning electron microscopy (SEM) images revealed carbon deposits with kerosene, reducing electrode wear by 87%, while deionized water caused 17% higher electrode wear than the graphene solution. Additionally, the graphene solution led to a 12% and 4% reduction in HAZ size compared to kerosene and deionized water, attributed to graphene’s high electrical conductivity. In summary, the graphene solution significantly increased MRR with a modest rise in electrode wear, improving hole quality and reducing thermal damage compared to kerosene and deionized water. Also, Kumaran et al. [25] found that adding fillers like carbon black (1 and 2 vol%) and graphite (5 and 10 vol%) to the CFRP matrix enhanced MRR, reaching up to  $4 \text{ mm}^3/\text{min}$  compared to  $2.2 \text{ mm}^3/\text{min}$  for reference CFRP. Additionally, tool wear and thermal damage near the hole exit were

reduced, likely due to the increased thermal conductivity of the matrix, which allowed heat to diffuse more effectively and prevented matrix degradation.

Furthermore, Yue et al. [26] conducted a comprehensive examination that revealed the presence of multiple material removal mechanisms during CFRP EDM, beyond thermal erosion induced by plasma and Joule heating. These mechanisms included the evaporation of epoxy resin and the sublimation of carbon fibres, generating high-speed gaseous jets. These jets contributed to material removal by breaking loose fibres following resin decomposition. Furthermore, a comparison of dielectric media revealed that deionized water yielded a higher MRR (0.6 mg/min) compared to oil-based dielectric (0.2 mg/min). This disparity was attributed to the presence of dissociated oxygen molecules produced from deionized water during the discharge process, enhancing overall thermal energy generation. Sheikh-Ahmed [17] further investigated the effects of varying current and pulse-on time on EDM drilling of CFRP, focusing on MRR and workpiece damage. The study identified key cutting mechanisms involving Joule heating, plasma-induced epoxy matrix disintegration, and fibre and epoxy matrix vaporization. Moreover, Park et al. [27] investigated micro-EDM for CFRP drilling, finding that MRR increased with higher discharge current, voltage, and pulse duration, while pulse frequency had minimal impact above 75 kHz. Increasing these parameters also consistently raised the tool wear ratio (TWR). Excess discharge energy caused significant surface damage, which could be mitigated by optimizing energy levels. Similarly, Kaushik et al. [28] studied the effects of voltage, capacitance, and tool rotation speed on MRR, roundness error, and taper in CFRP micro-EDM drilling. It was found that capacitance and voltage significantly influenced roundness error, with capacitance having the most impact on MRR and micro-hole quality.

However, Kumar et al. [29] addressed micro-EDM using different tool geometries, primarily solid and single/double notch configurations, across various capacitance, voltage, and rotation speed settings. Their findings highlighted the superiority of the single notch tool, achieving the highest MRR ( $1.854 \times 10^{-3} \text{ mm}^3/\text{min}$ ) and aspect ratio (29.17), along with an intermediate wear rate ( $9.45 \times 10^{-5} \text{ mm}^3/\text{min}$ ). Operating at 1500 rpm effectively enhanced MRR, while optimal surface quality was attained at a low discharge energy of 0.106  $\mu\text{J}$ . Their study demonstrated superior aspect ratios of 29.17 compared to previous research studies [30, 31]. To enhance micro-EDM performance, Dutta et al. [32] used thin copper foil (0.07 mm thick) as an assisted electrode and examined MRR and surface integrity by varying voltage, pulse duration, and tool speed. Their results showed that voltage had the most significant impact on MRR, with a percentage contribution ratio of 75.09%, followed by speed (16.09%) and pulse duration (5.2%). The optimal conditions

for maximum MRR were 170 V, 800 rpm, and 10  $\mu\text{s}$ . The assisted electrode (AE) was crucial for spark initiation, supported by a pyrolytic carbon layer from hydrocarbon oil breakdown, which facilitated continuous spark generation. However, the machined surface exhibited defects such as matrix burning and fibre spalling due to elevated heat generation. Additionally, the effect of silicon carbide powder concentration (4, 8, 12, and 16 g/l) in dielectric fluid (kerosene) on drilling blind square micro-holes using a 0.8-mm square copper electrode was investigated [33]. The study evaluated squareness, hole depth, surface roughness, electrode wear length, and surface defects. Results indicated that both SiC concentration and pulse duration significantly influenced all response measures. Irregular cutting edges and electrode wear at all machined corners were observed due to unstable discharging. Furthermore, the skin effect induced corner radii in the machined holes.

In an independent study, Islam et al. [34] investigated the deburring process of predrilled holes in CFRP. Their exploration focused on assessing the impact of altering capacitance and electrode materials, including copper, aluminium, steel, and brass, on MRR. Elevated MRRs were noted with higher capacitance, reaching the peak value of 6.3  $\text{mm}^3/\text{min}$  when utilizing a copper electrode. Conversely, the lowest MRR of 3.7  $\text{mm}^3/\text{min}$  was observed with aluminium, attributed to differences in electrical conductivity among the various electrode materials.

In another context, Lau and Lee [35] delved into wire EDM and compared its results with those of the laser cutting process in CFRP machining. Their study highlighted the effectiveness of both processes in machining CFRP, with a focus on MRR, cut-edge quality, and material damage. While laser cutting exhibited faster material removal (95  $\text{mm}^3/\text{min}$ ), WEDM (12  $\text{mm}^3/\text{min}$ ) offered superior control over process variables, resulting in reduced material damage and improved edge-cut profiles. Furthermore, Abdallah et al. [36] explored the effects of cut direction and process parameters, including open gap voltage, ignition current, pulse-on time, and pulse-off time, in WEDM of unidirectional CFRP (UD-CFRP) laminates. The study revealed that the highest MRR (2.41  $\text{mm}^3/\text{min}$ ) was achieved when cutting parallel to the fibre orientation, with ignition current and pulse-off time emerging as the most significant parameters. In contrast, perpendicular cutting to the fibre orientation resulted in lower MRR (2.08  $\text{mm}^3/\text{min}$ ), attributed to reduced electrical conductivity. This perpendicular cutting orientation also exhibited significant delamination along kerf edges and lower surface roughness. Also, Abdallah et al. [37] investigated the impact of wire electrode type (Topas Plus D and Compeed) on the WEDM machinability of multidirectional CFRP, assessing kerf widths, surface roughness, and material removal rates. Topas wire exhibited MRRs 11 to 40% higher than Compeed under identical conditions, reaching

maximum values of 14.82 mm<sup>3</sup>/min and 13.31 mm<sup>3</sup>/min, respectively. Pulse-off time was the sole parameter with statistical significance on MRR, contributing significantly. Various damages on machined surfaces, including delamination, uneven edges, adherent debris, fractured fibres, and resin buildup, were observed. Notably, Compeed induced more severe damage due to its higher electrical conductivity ( $29 \times 10^6$  S/m), resulting in wider kerf widths than Topas. Narrower kerf widths were achieved by increasing pulse-off time, reducing the interaction time between the discharge spark and the workpiece. Surface roughness measurements indicated greater roughness on surfaces machined with Compeed wire, attributed to increased heat generation from its higher electrical conductivity. In a separate study, Wu et al. [38] introduced a novel approach employing steel plates as assisted electrodes during the machining of unidirectional CFRP. This innovative technique aimed to improve the bulk electrical conductivity of CFRP. As a result, greater heat transfer to the wire was achieved, allowing it to melt the low-conductivity epoxy resin matrix present in CFRP effectively. Consequently, machining efficiency increased, preventing wire breakage during WEDM. The study conducted machining tests at various cut angles, resulting in reduced kerf widths and improved kerf straightness as cut angles increased, particularly over a 10-mm cut distance in all directions. However, typical WEDM damage, including expanded fibre tips, lingering resin, fused fibres, and debonding, was still evident on the machined surfaces. Similarly, Dutta et al. [39] and Anbalagan [40] demonstrated the effectiveness of using assisted electrodes like H13 steel plates and 409-grade stainless steel. They found that these electrodes prevented wire breakage, maintained the straightness of the cutting profile, and improved discharge performance. The findings showed a significant reduction in machining time by up to 60.95% and 59.80%, respectively, achieved by increasing current and reducing pulse-off time to 12 A and 10  $\mu$ s. Recently, the high-speed wire EDM (HS-WEDM) technique was employed to examine the impact of machining parameters, including pulse on/off times (Pon/Poff), current ( $I$ ), and plate thickness ( $T$ ) (0.5, 1.0, 1.5, and 2 mm), on corner inaccuracy (CI) at various angles (30°, 60°, 90°, and 120°) [41]. Multi-response optimization was performed to identify the optimal cutting conditions for different plate thicknesses. The results showed that Pon and  $T$  were the most influential parameters on CI at 30°, with PCR of 43.3% and 30.34%, respectively. Plate thickness had the most significant effect on CI at 60°, 90°, and 120°. For achieving precise corners at thicknesses of 0.5 and 1.0 mm, the optimal cutting conditions were 40  $\mu$ s (Pon), 15  $\mu$ s (Poff), and 4 A ( $I$ ). For thicknesses of 1.5 and 2 mm, the optimal conditions were 45  $\mu$ s (Pon), 30  $\mu$ s (Poff), and 2 A ( $I$ ).

In summary, recent research efforts have predominantly focused on using die-sink EDM for drilling thin samples,

micro-drilling, and deburring of CFRP, while wire EDM has mainly been used for linear cutting of CFRP. There is a lack of investigations and modelling into the application of WEDM for drilling holes in CFRP. Therefore, the novelty of this study lies in assessing the feasibility of using the WEDM technique for drilling thick CFRP materials and analytically predicting the temperature distribution during the cutting process.

## 2 Experimental work

### 2.1 Workpiece material, machining equipment, and analysis equipment

In this study, two square CFRP workpieces were employed, each measuring 100  $\times$  100 mm. The configurations comprised both unidirectional and multidirectional, with respective thicknesses of 8.4 mm and 9.36 mm. The multidirectional workpiece, classified as a type-2 laminate, had a density of 0.0016 g/mm<sup>3</sup> and consisted of 36 plies of carbon fibres pre-impregnated in an epoxy resin matrix. These plies were arranged in a specific sequence:  $[45^\circ/0^\circ/135^\circ/0^\circ/90^\circ/0^\circ/135^\circ/0^\circ/45^\circ]_{4S}$ , as detailed in Table 1. In contrast, the unidirectional workpiece plate had a density of 0.0018 g/mm<sup>3</sup> and was made up of 32 plies of intermediate modulus carbon fibres (294 GPa) that were pre-impregnated in an epoxy resin matrix. These fibres were manually aligned in the 0° fibre direction before undergoing autoclave curing to consolidate the laminates.

The experimental procedures were conducted on an AgieCharmilles Robofil FI240CC wire EDM machine, which was equipped with a CleanCut minimum damage generator, as illustrated in Fig. 1. Throughout the machining process, the workpiece was submerged in deionized water with a conductivity level of 5  $\mu$ S/cm. The tool electrode employed was a wire with a diameter of 0.25 mm, characterized by high tensile strength (800 MPa). This wire featured a steel core enveloped by a dual layer consisting of copper and a diffused-phase brass coating, offering an electrical conductivity of  $29 \times 10^6$  S/m. A previous study [37] confirmed that this wire exhibited remarkable rigidity and exceptional resistance to breakage due to its high-strength properties, contributing significantly to the stability of the cutting process.

**Table 1** No of plies corresponding to each fibre orientation angle (multidirectional)

Fibre orientation angle	No. of plies
0°	16
45°	8
90°	4
135°	8

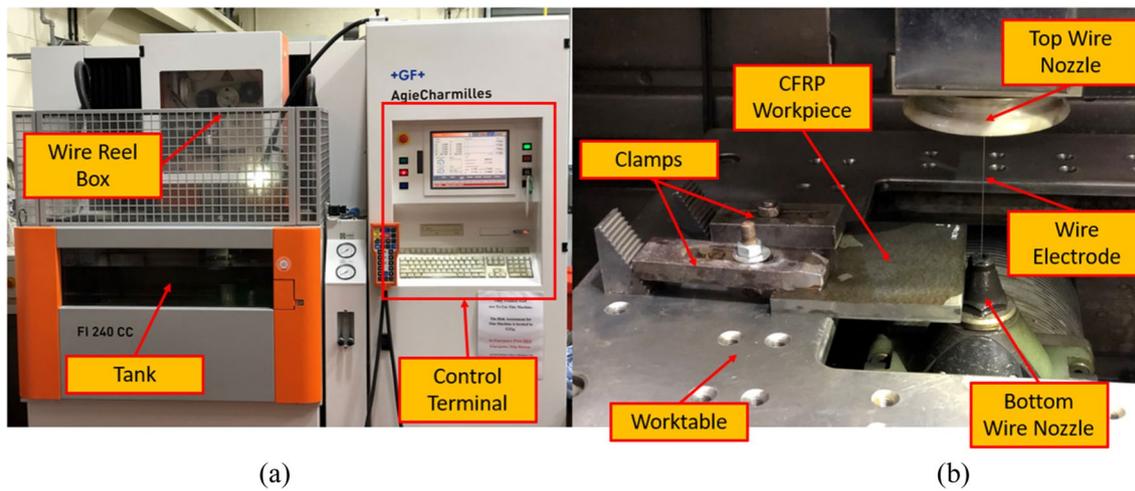


Fig. 1 AgieCharmilles Robofil FI240CC: **a** machine tool and **b** experimental setup

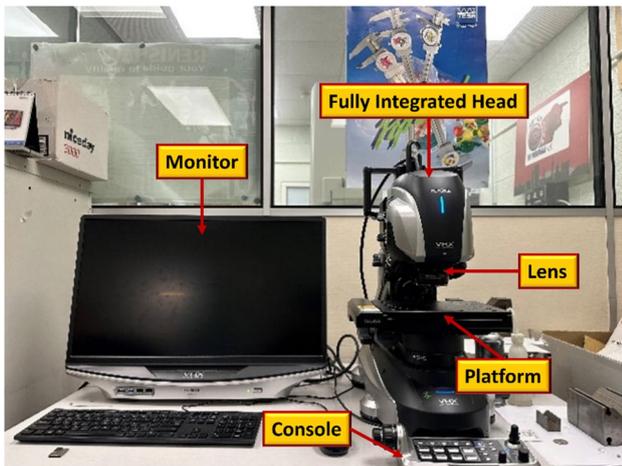


Fig. 2 Keyence VHX-7000 digital microscope

Following each machining trial, an air blower and a hair dryer were utilized to facilitate the drying and evaporation of any absorbed water within the CFRP plates. Subsequently, the mass of the workpiece was determined using a digital scale characterized by a measurement range spanning from 0.5 to 3500 g and a precision level of 0.001 g. The top and bottom surfaces of the drilled holes were examined utilizing the Keyence VHX-7000 digital microscope, employing magnification levels ranging from  $\times 50$  to  $\times 80$ , as depicted in Fig. 2. In the subsequent analysis, the VHX analysis programme’s optical shadow effect mode was employed to assess surface damage and drilled holes diameter.

Table 2 Variable and fixed parameters

Machining parameters		Levels	
		1	2
Variable	Ignition current, IAL (A)	3	5
	Pulse-off time, B ( $\mu$ s)	4	6
	Material lay-up	Unidirectional	Multi-directional
Fixed	Open gap voltage, Vo (V)	120	-
	Servo voltage, Aj (V)	20	-
	Wire tension, WB (N)	13	-
	Wire speed, WS (m/min)	10	-
	Flushing pressure, INJ (bar)	16	-
	Frequency, FF (%)	10	-
	Pulse-on time, A ( $\mu$ s)	0.8	-

## 2.2 Experimental design and test procedures

Through preliminary trials, it was observed that varying the ignition current and pulse-off time are essential parameters for achieving successful cutting. To investigate these variables, a comprehensive experimental design was employed, utilizing a full factorial approach that encompassed variable factors mainly ignition current and pulse-off time each at two levels while maintaining a constant set of parameters, including open gap voltage, servo voltage, wire tension, wire speed, flushing pressure, frequency, and pulse-on time, as outlined in Table 2. A total of eight tests were executed, evenly divided between unidirectional and multidirectional CFRP plates, as delineated in Table 3, representing the full factorial orthogonal array applied in this study. Each test involved

**Table 3** Experimental test array

Test no	Ignition current, IAL (A)	Pulse-off time, B (μs)	lay-up
1	3	4	Unidirectional
2	5	4	Unidirectional
3	3	6	Unidirectional
4	5	6	Unidirectional
5	3	4	Multidirectional
6	5	4	Multidirectional
7	3	6	Multidirectional
8	5	6	Multidirectional

the precision drilling of a 3-mm diameter hole, during which the machining time was meticulously recorded using a stopwatch. Furthermore, before and after each test, the weight of the workpiece was accurately measured, facilitating the subsequent calculation of the material removal rate (MRR) according to Eq. 1 [36]

$$MRR = \frac{mb - ma}{\rho \times t} \tag{1}$$

In the given equation, *mb* signifies the initial mass of the workpiece before machining (measured in grammes), *ma* indicates the mass of the workpiece after machining (measured in grammes),  $\rho$  represents the density of the workpiece (measured in g/mm<sup>3</sup>), and *t* denotes the machining time (measured in minutes).

The delamination factor (DF) as a result of the damage on the top and bottom faces of the workpiece was calculated using Eq. 2 [42].

$$DF = \frac{D_{max}}{D_n} \tag{2}$$

where  $D_{max}$  represents the largest delamination diameter observed, while  $D_n$  corresponds to the nominal diameter of the drilled hole.

The analysis of variance (ANOVA) was conducted to assess the significance of parameters on response measurements. This analysis was carried out using Minitab 20 statistical software with a confidence interval of 95%.

### 2.3 Thermal distribution modelling

The differential equation of heat transfer can be stated analytically and with consideration for the external heat sources as follows [43]:

$$\rho c_p \frac{dT_i}{dt} = \nabla(k\nabla T) + Q \tag{3}$$

where *k* (W/mK) is the thermal conductivity,  $\rho$  is the density (kg/m<sup>3</sup>),  $c_p$  is the specific heat capacity (J/kgK), *T* (K) is the temperature, and *Q* is the heat source (W/m<sup>2</sup>).

To determine the surface temperature of the specimen, a derived analytical solution for the partial differential equation (PDE) in an adiabatic setting was undertaken, where there is no heat exchange through convection or radiation with the surroundings. Consequently, the resulting 1-D analytical solution exclusively showcases pure heat conduction and is very applicable to the case of carbon fibres since they are considered 1-D elements due to their infinitesimal radius, compared to their length. This analytical solution is used for delineating the heating and cooling stages during a singular discharge spark, and it is assumed that the material starts at 300 K (room temperature) when *t*=0, and the temperature at *z*=∞ remains consistently at room temperature for *t*>0.

The intensity of the heat source is determined by dividing the spark power by the spark radius, taking into account additional process factors. These factors include the cathode energy fraction, representing the proportion of heat source energy absorbed by the workpiece, and the plasma flushing efficiency, which defines the ratio between the actual machined material and the theoretically removed amount by a single spark. Consequently, the heat generated during EDM can be computed as follows:

$$Q = \frac{I \times V \times F_c \times \eta}{\pi r_s^2} \tag{4}$$

where *I* is the discharge current (A), *V* is the discharge voltage (V),  $F_c$  is the cathode energy fraction,  $r_s$  is the plasma channel radius (m), and *Q* is the heat source (W/m<sup>2</sup>).

The plasma channel radius (m) is usually very difficult to estimate; however, Assarzadeh and Ghoreishi [44] provided an estimate of its value depending on the discharge current and time:

$$r_s = 2040 \times 10^{-6} \times I^{0.43} \times t_{on}^{0.44} \tag{5}$$

Considering the aforementioned assumptions, a modified form of the analytical solution produced by Alshaer et al. [43] is now applied as two sets of equations to describe the heating and cooling phases.

$$T(z, t)|_{t < t_{on}} = T_0 + \frac{2Q}{k} \sqrt{D \times t} \left( \text{ierfc} \left[ \frac{z}{2\sqrt{D \times t}} \right] \right)$$

$$T(z, t)|_{t > t_{on}} = T_0 + \frac{2Q}{k} \left( \sqrt{D \times t} \text{ierfc} \left[ \frac{z}{2\sqrt{D \times t}} \right] - \sqrt{D(t - t_{on})} \text{ierfc} \left[ \frac{z}{2\sqrt{D(t - t_{on})}} \right] \right)$$

where *z* is the depth at which the temperature is calculated,  $T_0$  is the initial temperature,  $I_0$  is the heat source, *D* is the

thermal diffusivity ( $k/\rho c_p$ ),  $t_{on}$  is the discharge time ( $0.8 \mu s$ ),  $t$  is the time, and  $ierfc$  is the error function.

In the analysis, the process parameters and material properties utilized are outlined in Table 4.

### 3 Results and discussion

#### 3.1 Material removal rate

The machining trials for drilling 3-mm holes produced machining times ranging from 64 to 104 min for unidirectional lay-ups and 26 to 93 min for multidirectional lay-ups. The extended machining time is attributed to the thick workpiece material and the different machining behaviour for both lay-ups which impacts both flushing and discharging performance. Figure 3 shows the effect of varying ignition current and pulse-off time on the MRR when cutting unidirectional and multidirectional CFRP laminates, using the Compeed wire electrode. MRR for the multidirectional lay-up was noted to be significantly higher compared to the unidirectional lay-up for all tests at equivalent parameters.

**Table 4** Material properties and process parameters used in the analytical solution [45–48]

Variable	Value	Variable	Value
$I$	3 and 5 A	$t_{on}$	$0.8 \mu s$
$V$	120 V	$\rho$	$1875 \text{ kg/m}^3$
$F_c$	8%	$k$	$1000 \text{ W/mK}$
$\eta$	100%	$c_p$	$1150 \text{ J/kgK}$
Carbon fibre $T_m$	$3947.5 \text{ K}$	Carbon fibre $T_v$	$4473 \text{ K}$
Epoxy $T_m$	$448.5 \text{ K}$	Epoxy $T_v$	$525 \text{ K}$

The maximum MRR values for multidirectional and unidirectional CFRP laminates recorded were  $2.85 \text{ mm}^3/\text{min}$  (test 6) and  $0.95 \text{ mm}^3/\text{min}$  (test 2), respectively. Both laminates recorded the highest MRR with ignition current at 5 A and pulse-off time at  $4 \mu s$  which was attributed to the higher discharge energy. Although there is a lack of research on drilling CFRP using WEDM configuration, these findings are consistent with other studies on linear cutting of CFRP, which confirm that the highest MRR is achieved at the highest current (5 A) and the lowest pulse-off time ( $4 \mu s$ ) [36]. Similarly, die-sink EDM studies have shown the highest MRR of up to  $30 \text{ mm}^3/\text{min}$  at the highest current of and a pulse-on time when drilling various hole diameters and thicknesses of CFRP [8, 49]. The highest MRR for multidirectional CFRP was 300% greater than that for unidirectional CFRP. Additionally, the main effect plot for the mean MRR clearly indicates that MRR increases with higher ignition current and lower pulse-off times. Overall, the multidirectional lay-up exhibited significantly higher MRR compared to the unidirectional lay-up, as shown in Fig. 4.

This is likely attributed to the diversity in interaction behaviour between the wire electrode and CFRP laminate. In a unidirectional lay-up, the interaction of the electrode with the matrix is dependent on the fibres and the electrode feeding directions, which leads to a different material behaviour; hence, non-uniformity would be expected due to the variable contact, as discussed in the next subsection. This behaviour however is absent in the case of multidirectional CFRP because the electrode will have approximately similar contact regardless of the feeding direction as depicted in Fig. 5. Hence, more consistent drilling and MRR will be expected in this case at the same cutting conditions.

Carbon fibres and the resin electrical resistivity were measured at  $158\text{--}501$  and  $1022 \mu\Omega \times \text{cm}$ , respectively [22].

**Fig. 3** Comparison between material removal rates of different lay-ups at the same cutting conditions

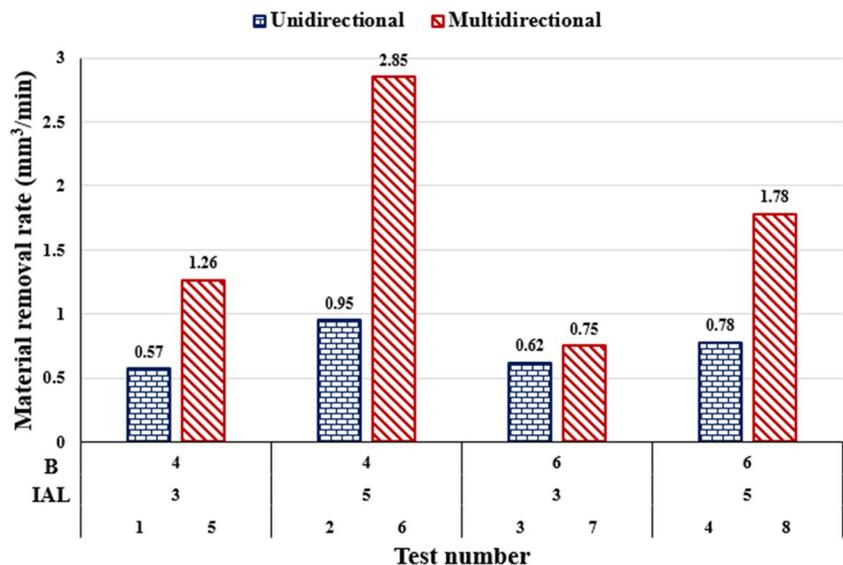


Fig. 4 Main effect plot for MRR

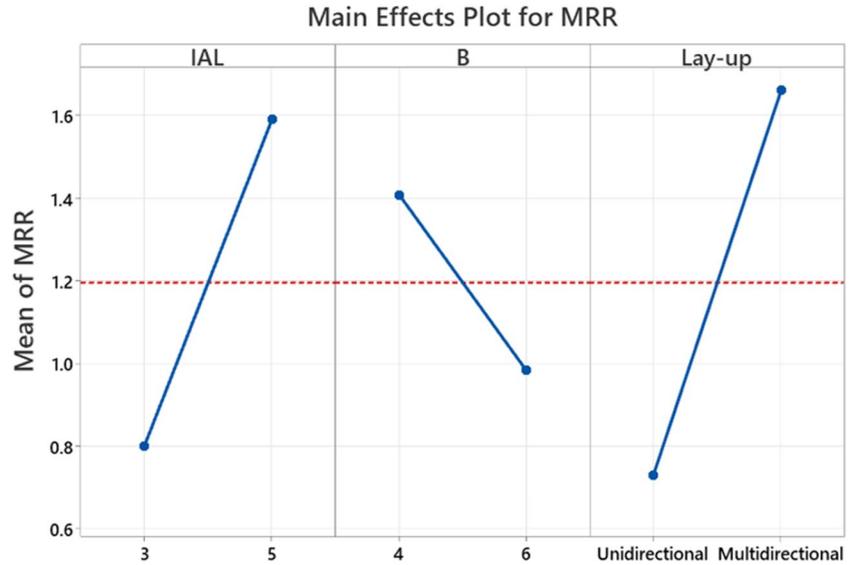
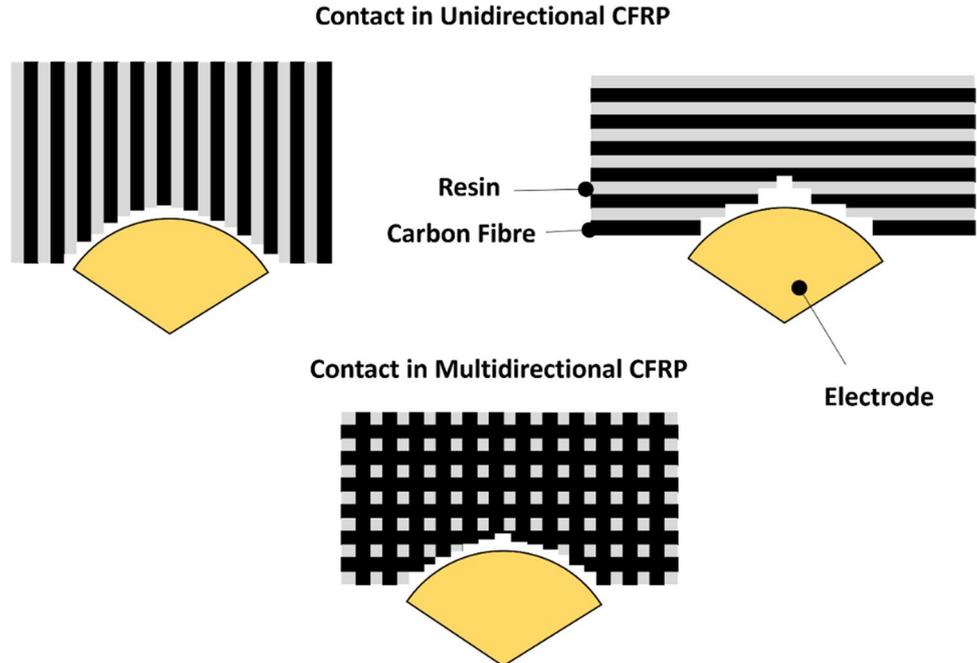


Fig. 5 Contact between the electrode and unidirectional and multidirectional CFRP [22]



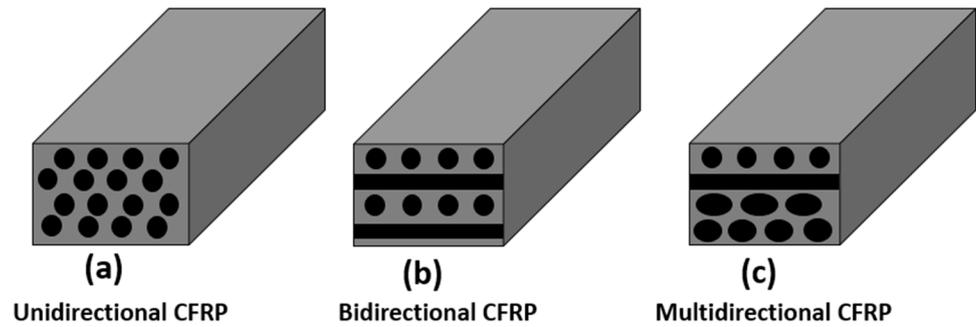
Hence, cross sections with larger fibre content will receive a larger portion of discharge energy compared to the resin/epoxy-rich sections. Figure 6 clearly shows that the fibre-rich area in the multidirectional CFRP cross section is larger than the unidirectional, and the electrical discharge would therefore act on a larger area compared to the unidirectional section, and more heat would be generated and conducted to the resin and other neighbouring fibres.

Table 5 presents the analysis of variance (ANOVA), incorporating several acronyms: DF (degree of freedom), representing the number of independent variables; Seq SS (sequential sum of squares), measures total variation; Adj SS

(adjusted sum of squares), measuring variation after model adjustments; and Adj MS (adjusted mean squares), Adj SS divided by DF. The  $F$ -value tests the factor significance on the response variable, while the  $p$ -value indicates the probability of results under the null hypothesis. A  $p$ -value  $\leq 0.05$  typically suggests strong evidence against the null hypothesis. PCR % (percentage contribution ratio) identifies the most impactful factors.

The analysis revealed that all parameters and interactions exhibited  $p$ -values exceeding 0.05, indicating their lack of significance in the observed responses; however, the lay-up demonstrated the highest percentage contribution ratio

**Fig. 6** Fibre area in different lay-up cross sections: **a** unidirectional, **b** bidirectional, and **c** multidirectional CFRP laminates



**Table 5** Analysis of variance of material removal rate

Source	DF	Seq SS	Adj SS	Adj MS	F-value	p-value	PCR %
Model	6	4.22255	4.22255	0.70376	48.70	0.109	99.66%
Linear	3	3.33925	3.33925	1.11308	77.03	0.084	78.81%
IAL	1	1.24820	1.2482	1.2482	86.38	0.068	29.46%
B	1	0.36125	0.36125	0.36125	25.00	0.126	8.53%
lay-up	1	1.72980	1.72980	1.7298	119.71	0.058	40.83%
2-way interactions	3	0.8833	0.8833	0.29443	20.38	0.161	20.85%
IAL*B	1	0.07605	0.07605	0.07605	5.26	0.262	1.79%
IAL*lay-up	1	0.5408	0.5408	0.5408	37.43	0.103	12.76%
B*lay-up	1	0.26645	0.26645	0.26645	18.44	0.146	6.29%
Error	1	0.01445	0.01445	0.01445			0.34%
Total	7	4.237					100.00%
Model summary							
S	R-sq	R-sq (adj)		R-sq (Pred)			
0.120208	99.66%	97.61%		78.17			

(PCR) of 40.83% followed by 29.64% and 8.53% for ignition current and pulse-off time, respectively, see Table 5. This insignificance can be primarily attributed to the considerable variability observed in machining times and material removal rates (MRR) across both lay-ups of CFRP. This variability stems from the material’s anisotropic nature, which leads to differential heat generation influenced by varying fibre orientations. This behaviour complicates resin matrix decomposition during machining, resulting in unstable spark intensities [22, 36]. Moreover, the machining of thick workpiece materials hindered effective debris flushing from the machining gap, further impacting spark intensity and consequently prolonging machining times. While the multidirectional lay-up exhibited greater consistency during cutting, as depicted in Fig. 5, the inclusion of results from the unidirectional lay-up introduced additional variability into the overall analysis. In comparison with the WEDM drilling of various CFRP lay-ups, linear WEDM studies conducted by Abdallah et al. [36, 37, 50] underscored the significant influence of machining parameters on MRR. They highlighted the advantages of consistent cutting and the closer alignment of test results obtained through single-direction cutting versus simultaneous cutting in both x and

y directions during drilling processes. The derived regression model showed strong agreement with the experimental data and likely included all the relevant terms for good correlation between the response and machining variables for both multidirectional and unidirectional CFRP, based on the coefficient of determination ( $R^2$ ) of 99.66% and an adjusted coefficient of determination (Adj  $R^2$ ) of 97.61%.

### 3.2 Surface damage

Optical micrographs of the top and bottom surfaces of the machined holes for the unidirectional and multidirectional CFRP plates in each test are tabulated in Table 6. All tests showed surface defects such as frayed fibres, resolidified resin, adhered debris, and varying levels of delamination. The top surfaces of both lay-up configurations exhibited considerable damage, particularly in the multidirectional CFRP, where severe damage and uncut or frayed fibres were observed at a high current of 5 A as depicted in test 8. This damage is primarily attributed to the high-speed gaseous jets produced by the decomposition and evaporation of the resin matrix, the sublimation of carbon fibres, and the collapse of plasma. Once the resin-rich areas evaporated, the carbon

**Table 6** Micrographs of the top and bottom surfaces of machined holes at different cutting conditions

Test no	Machining parameters			Drilled surface micrographs		Coloured texture map	
	Lay-up ( $\mu$ s)	B ( $\mu$ s)	IAL (A)	Top	Bottom	Top	Bottom
1	Unidirectional	3	3				
4		5	3				
2		6	3				
3		5	3				
4	Multidirectional	3	3				
4		5	3				
5		6	3				
6		5	3				
7	6	3					
8	5	3					

fibres became loose and were susceptible to breakage due to these high-speed jets, resulting in uncut fibres and extensive delamination [17, 26]. The coloured textured maps assist in better visualizing the extent of thermal damage induced by the spark in each test by increasing the saturation of red colour in regions with higher levels of thermal damage along the circumference of the machined holes.

As expected, thermal damage is more pronounced in the unidirectional composite with a shorter pulse-off time, whereas the difference is less significant in the multidirectional panel due to enhanced thermal conductivity resulting from a higher graphite content in the cross section. The multidirectional panel exhibits consistent in-plane thermal conduction, ensuring uniform heat flow—an aspect absent in the unidirectional lay-up. In terms of the hole profile, it is noted that using less discharge current improved the circularity of the holes for both lay-ups due to the reduction of the thermal damage produced using 5 A, compared to 3 A. Moreover, the multidirectional lay-up demonstrated better hole circularity compared to the unidirectional lay-up due

to the consistent thermal conductivity in the in-plane x and y direction.

The pulse-off time did not have any considerable influence on circularity in the multidirectional panels. However, longer pulse-off times clearly improved hole roundness in unidirectional lay-ups, especially at low current levels (3 A). Conversely, a notable deterioration in circularity was observed at high current levels and short pulse-off times due to the high discharge energy and anisotropic characteristics of the unidirectional lay-up. This clearly indicates that allowing longer relaxing time helps fibres and the matrix to reduce their temperature and dissipate heat before the next cycle of heating starts, hence reducing thermal damage caused by accumulative heating.

Figure 7 shows optical micrographs of the machined holes using optical and shaded effect modes on the top and bottom surfaces for unidirectional CFRP in test 2, which recorded the highest MRR. The top surface of the workpiece showed severe delamination along the circumference of the machined hole together with irregular/

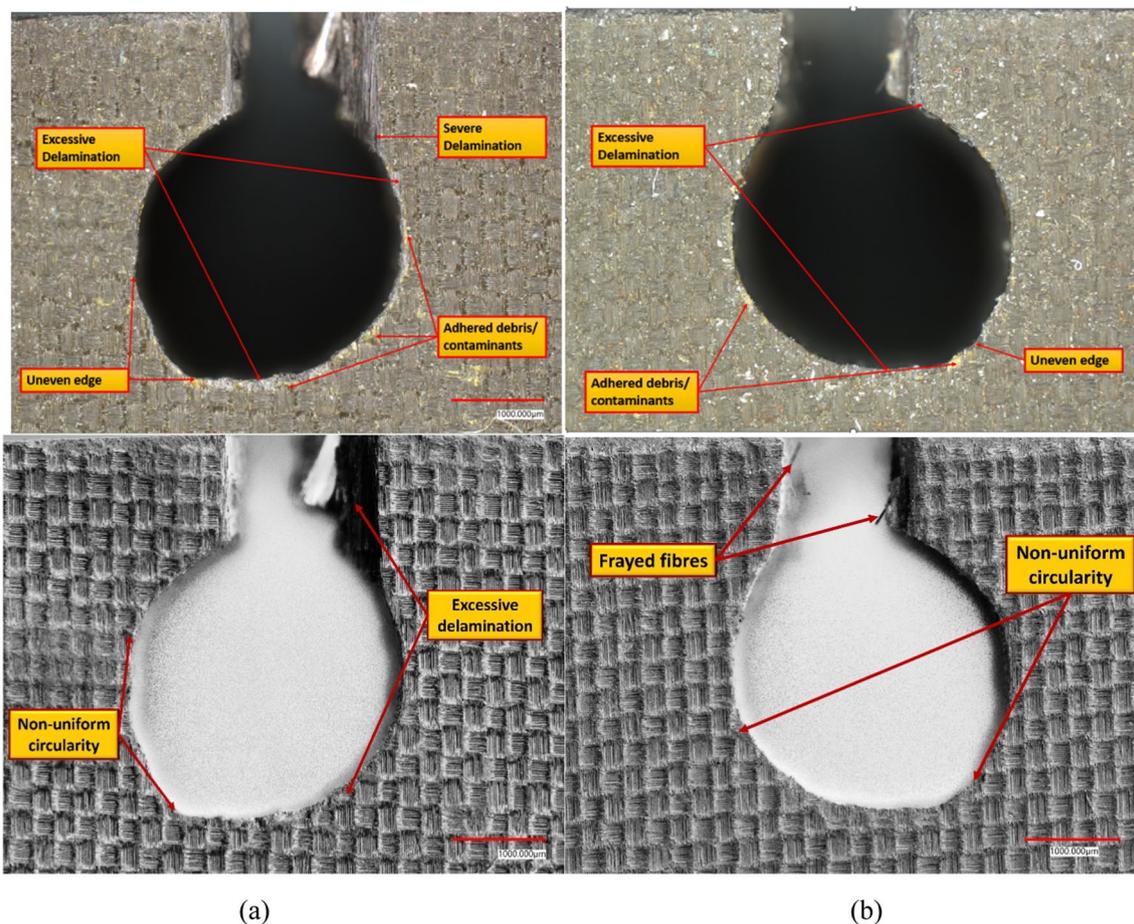


**Fig. 7** Micrographs illustrating the damage induced in unidirectional CFRP during test no. 2 (Max MRR) on both **a** top and **b** bottom surfaces using original and shaded modes

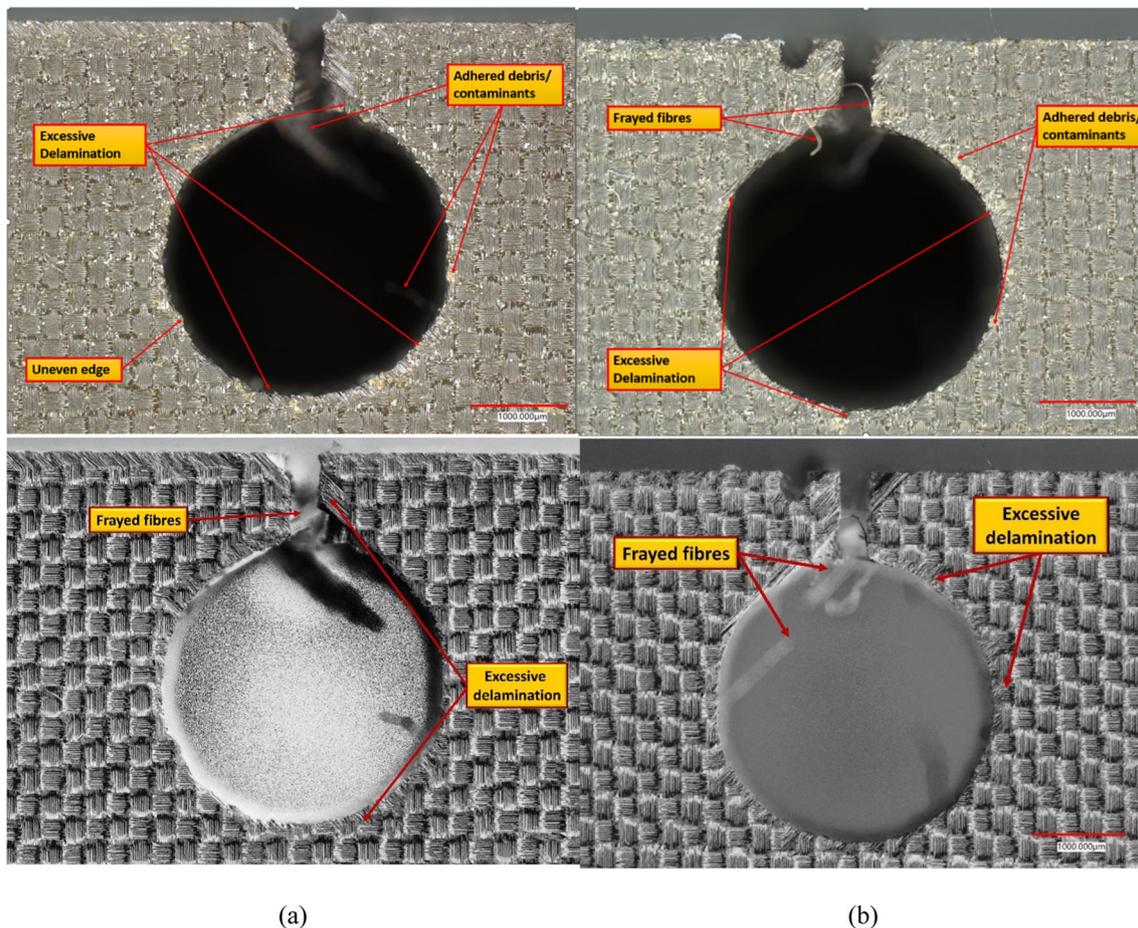
uneven circularity and the presence of frayed fibres and bronze-coloured debris, see Fig. 7a. The bottom surface also showed similar damage albeit to a lower degree as depicted in Fig. 7b. Due to the pressure of gases created by resin decomposition, delamination often occurs in epoxy-rich areas [17]. Combined with the non-uniform electrode-matrix interaction in the unidirectional composite, the gases, in conjunction with wire tension and electrostatic and dielectric cleansing forces, caused wire vibration, which most likely contributed to the irregular/uneven circularity. Furthermore, the observed fractured/frayed fibre damage was partly attributed to the impact of high-speed gaseous jets created during the vaporization and sublimation of epoxy/carbon fibres [26].

Similarly, Fig. 8 shows optical micrographs of the top and bottom surfaces of machined holes obtained at the highest MRR (test no. 6) during machining multidirectional CFRP. The top surface showed regions of high delamination along the circumference of the machined hole, see Fig. 8a and b. The circumference of the hole was also irregular/uneven

**Table 7** Top and bottom delamination factors

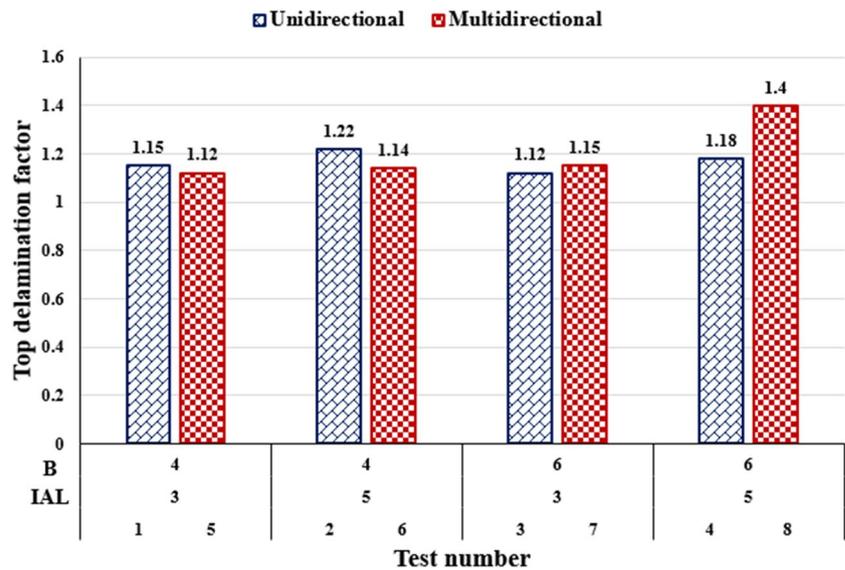
	Test no	Top	Bottom
Unidirectional	1	1.15	1.14
	2	1.22	1.19
	3	1.12	1.04
	4	1.18	1.24
Multidirectional	5	1.12	1.15
	6	1.14	1.15
	7	1.15	1.16
	8	1.4	1.13

with the presence of adhered debris/contaminants on the surface in an approximately 700- $\mu\text{m}$  radius around the hole. Similar damage was observed on the bottom surface alongside the presence of frayed fibres; however, the extent of damage was comparatively lower. Overall, at equivalent parameters, unidirectional CFRP showed more surface damage than multidirectional CFRP.



**Fig. 8** Micrographs illustrating the damage induced in multidirectional CFRP during test no. 6 (Max MRR) on both **a** top and **b** bottom surfaces using original and shaded modes

**Fig. 9** Top delamination factors for different lay-ups at the same cutting conditions



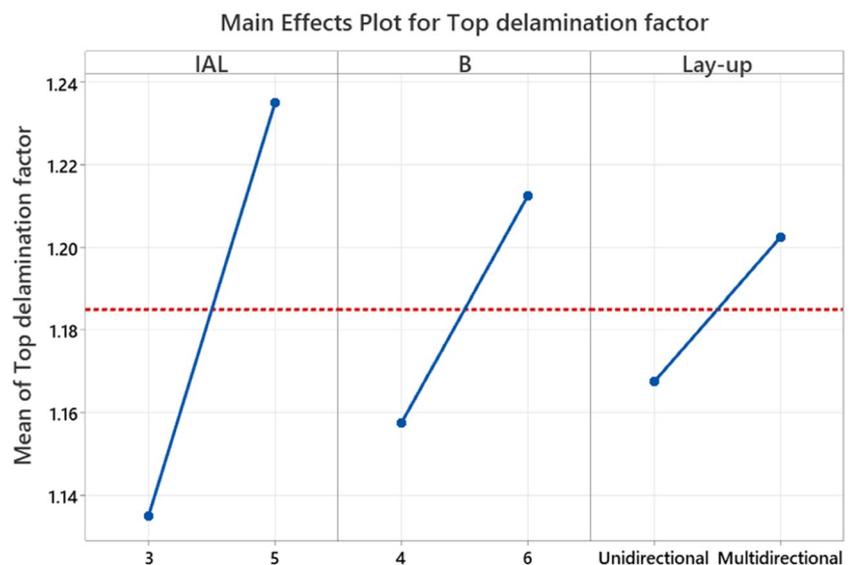
### 3.3 Delamination factor

Table 7 shows the calculated results for the top and bottom delamination factor values for both unidirectional and multidirectional CFRP. The results indicated that the top delamination factor increased as the ignition current rose from 3 to 5 A for both lay-up configurations, regardless of the pulse-off time. This confirms findings from other studies that increasing the current leads to higher delamination factors [8, 17]. Figure 9 demonstrates that the highest top surface delamination factor values were 1.22 (test 2) for the unidirectional CFRP and 1.40 (test 8) for the multidirectional CFRP at the high current level. For the unidirectional lay-up, higher top delamination factor values were observed at a low pulse-off time (4  $\mu$ s) compared to 6  $\mu$ s, particularly

at 5 A. This is attributed to the higher discharge energy, which exacerbated the anisotropic characteristics, leading to increased thermal damage and delamination. Additionally, insufficient cooling due to the low pulse-off time resulted in heat accumulation and resin decomposition, causing easier separation of fibre plies [36, 51]. In contrast, when machining the multidirectional CFRP lay-up, a significantly higher delamination factor was observed at extended pulse-off times (6  $\mu$ s). This trend can be attributed to enhanced debris removal from the machining gap due to effective flushing and intensified sparking during the pulse-on period. This combination increased the aggression of material removal, resulting in a higher level of delamination.

Overall, the main effect plot for the top surface delamination factor (see Fig. 10) demonstrated a clear increase in

**Fig. 10** Main effect plot for top delamination factor



**Table 8** Analysis of variance for top delamination factor

Source	DF	Seq SS	Adj SS	Adj MS	F-value	p-value	PCR %
Model	6	0.0532	0.0532	0.008867	1.23	0.598	88.08%
Linear	3	0.0285	0.0285	0.0095	1.32	0.552	47.19%
IAL	1	0.02	0.02	0.02	2.78	0.344	33.11%
B	1	0.00605	0.00605	0.00605	0.84	0.528	10.02%
lay-up	1	0.00245	0.00245	0.00245	0.34	0.664	4.06%
2-way interactions	3	0.0247	0.0247	0.008233	1.14	0.581	40.89%
IAL*B	1	0.00605	0.00605	0.00605	0.84	0.528	10.02%
IAL*lay-up	1	0.00245	0.00245	0.00245	0.34	0.664	4.06%
B*lay-up	1	0.0162	0.0162	0.0162	2.25	0.374	26.82%
Error	1	0.0072	0.0072	0.0072			11.92%
Total	7	0.0604					100.00%
Model summary							
S	R-sq		R-sq (adj)			R-sq (Pred)	
0.0848528	88.08%		16.56%			0.00%	

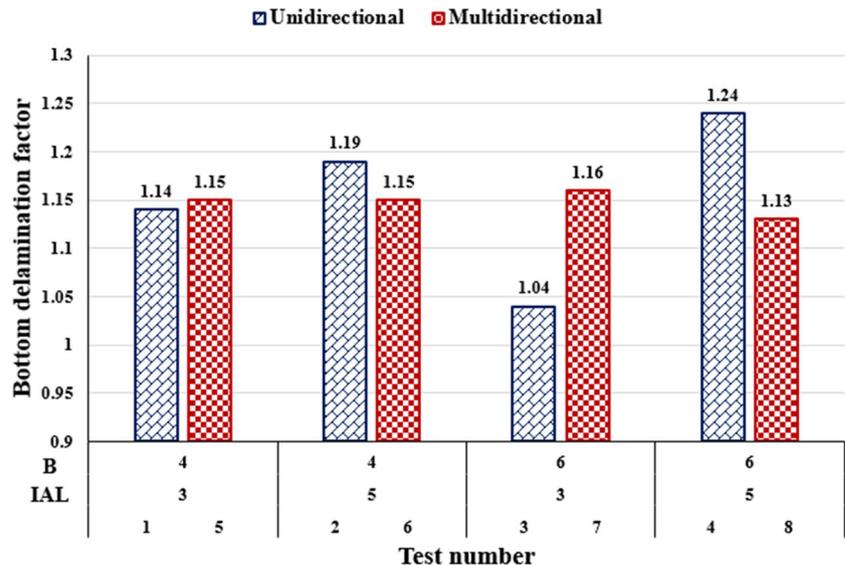
the delamination factor with higher ignition current and extended pulse-off time, consistent with the trend observed in the multidirectional lay-up in Fig. 9.

Table 8 details the ANOVA considering the effect of the main factors as well as the interactions between the parameters on the top surface delamination factor. In the ANOVA analysis, none of the parameters showed significance concerning the top delamination factor. This is attributed to the variability of findings across different lay-up configurations which exhibited different trends at various pulse-off time levels as a result of complex material structure alongside the anisotropic characteristics leading to the inconsistent effect of machining parameters on the response. Additionally, variations in the measurements of maximum delamination and hole diameters can introduce noise into the experimental outcomes. Nevertheless, ignition current demonstrated the

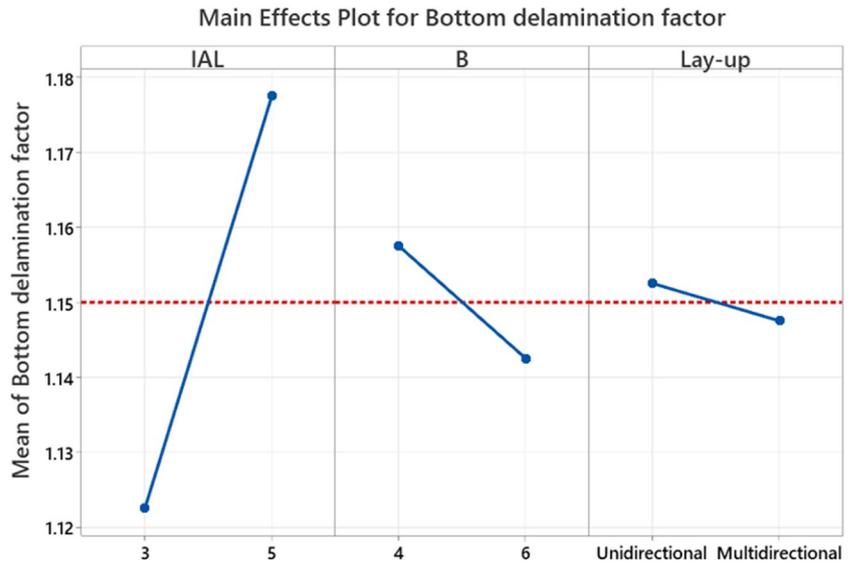
highest PCR at 33.11%, followed by 26.82% for the interaction between pulse-off time and lay-up. The results showed an  $R^2$  of 88.08%, which suggested strong agreement of the regression model with the experimental results; however, the small value of adjusted  $R^2$  (16.56%) indicates that the current model requires additional predictors to enhance the model's fitting.

Based on Fig. 11, the bottom delamination factors of both lay-up configurations exhibited contrasting trends compared to their respective top values. At a pulse-off time of 4  $\mu$ s, the unidirectional lay-up showed increasing delamination factor values with higher current, while the multidirectional lay-up maintained a consistent value of 1.15. Increasing the pulse-off time to 6  $\mu$ s resulted in the unidirectional lay-up reaching its peak value of 1.24 (test 4) at 5 A, whereas the multidirectional lay-up peaked at 1.16 (test 7) with a current

**Fig. 11** Bottom delamination factors for different lay-ups at the same cutting conditions



**Fig. 12** Main effect plot for bottom delamination factor



of 3 A. The main effect plot for the bottom surface delamination factor (see Fig. 12) indicated a noticeable increase in the delamination factor with higher ignition current and shorter pulse-off time for the unidirectional lay-up. Unlike the top delamination, the bottom surface exhibited opposite trends concerning pulse-off time and lay-up configuration. Overall, distinct delamination patterns were observed between the top and bottom surfaces, with the top surface consistently showing higher delamination values. These differences can be attributed to the anisotropic and non-homogeneous properties of CFRP materials, along with variations in thermal distribution across the thickness of the workpiece. Furthermore, the effectiveness of debris flushing leading to intense sparks on the top surface contrasts with poor flushing and debris accumulation affecting spark stability and intensity on the bottom surface, thereby resulting in less delamination.

Table 9 details the ANOVA considering the effect of the main factors as well as the interactions between the parameters on the bottom surface delamination factor. Similarly, all individual parameters and their interactions showed no significant effect on the bottom delamination factor. This is likely due to the inconsistent cutting behaviour caused by the anisotropic characteristics of the different lay-ups, as well as variability in the workpiece material itself and different material removal mechanisms, which introduced noise into the outcomes. According to the results, ignition current recorded the highest PCR of 27.01%, followed by pulse-off time at 2.01% and lay-up at 0.22%. The findings showed an  $R^2$  of 81.92% and an Adj  $R^2$  of 0%, which suggested strong agreement of the regression model with the experimental results; however, it suggests that additional parameters or process adjustments are needed to optimally control the delamination factor values.

**Table 9** Analysis of variance for bottom delamination factor

Source	DF	Seq SS	Adj SS	Adj MS	F-value	p-value	PCR%
Model	6	0.01835	0.01835	0.003058	0.76	0.706	81.92%
Linear	3	0.00655	0.00655	0.002183	0.54	0.734	29.24%
IAL	1	0.00605	0.00605	0.00605	1.49	0.437	27.01%
B	1	0.00045	0.00045	0.00045	0.11	0.795	2.01%
lay-up	1	0.00005	0.00005	0.00005	0.01	0.930	0.22%
2-way interactions	3	0.0118	0.0118	0.003933	0.97	0.615	52.68%
IAL*B	1	0.0018	0.0018	0.0018	0.44	0.626	8.04%
IAL*lay-up	1	0.0098	0.0098	0.0098	2.42	0.364	43.75%
B*lay-up	1	0.0002	0.0002	0.0002	0.05	0.861	0.89%
Error	1	0.00405	0.00405	0.00405			18.08%
Total	7	0.0224					100.00%
Model summary							
S		R-sq		R-sq (adj)		R-sq (Pred)	
0.0636396		81.92%		0.00%			0.00%

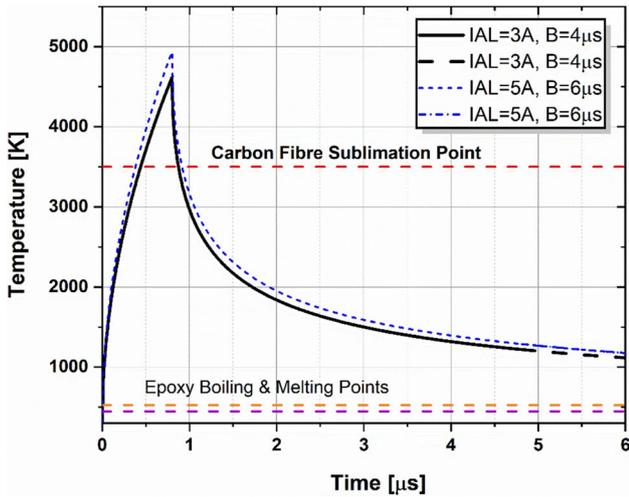


Fig. 13 Temperature variation with time for a single spark using 0.8- $\mu$ s discharge time with different current and pulse-off times

### 3.4 Thermal distribution

It is clear from Fig. 13 that the temperature generated in a single spark is adequate to vaporize the fibres and the resin, due to heat conduction, within only 0.8- $\mu$ s discharge time. The temperature decreases when discharge is completed, and the temperature drops significantly below the melting point of the fibres but still higher than the resin’s flash points. At the end of the cooling time of 4  $\mu$ s or 6  $\mu$ s, another spark appears, and the temperature rises again, and more material is machined. It must be noted that higher cathode energy fraction will cause the temperature to

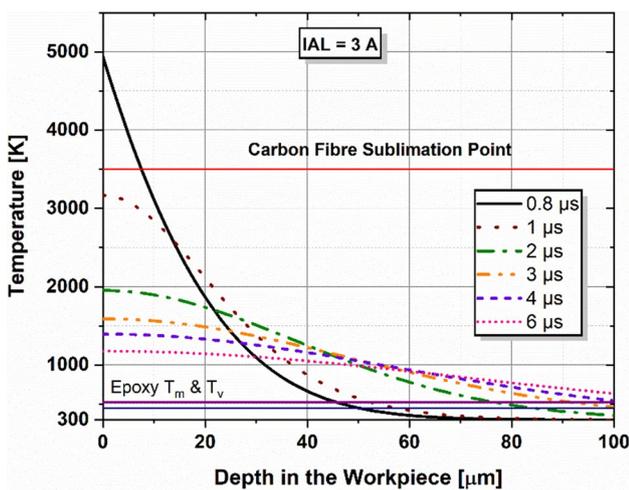


Fig. 14 Temperature distribution across the depth of the workpiece using IAL of 3 A at different times

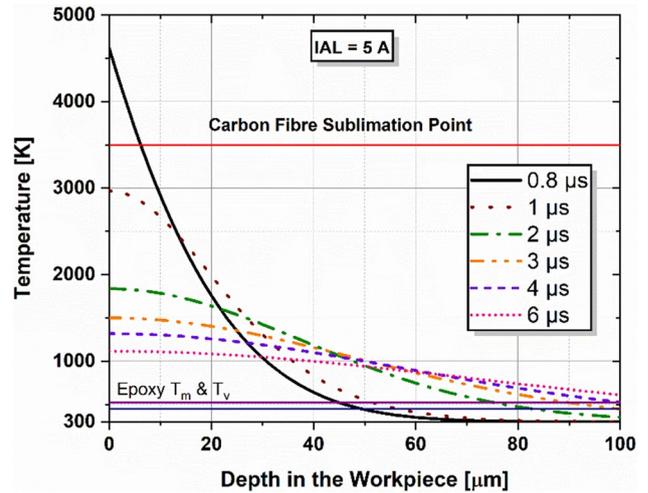


Fig. 15 Temperature distribution across the depth of the workpiece using IAL of 5 A at different times

significantly increase and guarantee the vaporization of the fibres. Moreover, longer cooling periods ( $B = 6 \mu$ s) allow the temperature to drop more, and hence, more time is required to increase the temperature again, hence causing the MRR to drop compared to shorter off-time such as 4  $\mu$ s.

Figures 14 and 15 show the temperature distribution across the depth of the workpiece using different discharge currents at different times. It is clear that just at the end of the discharging time of 0.8  $\mu$ s, the temperature at the surface is maximum at around 4990 K while it drops to the room temperature (300 K) at around 70  $\mu$ m, i.e. the heat is conducted in the fibres to a distance of 70  $\mu$ m away from the surface. The furthest distance at which the resin temperature exceeds the flash point at 0.8  $\mu$ s is around 45  $\mu$ m from the surface of machining, indicating that 45  $\mu$ m of the epoxy matrix is removed. This correlates well with the estimated thermal damage and delamination thickness of around 30–50  $\mu$ m, as shown in Table 5 and Figs. 7 and 8. It is important that this value is not always constant due to the variation in the real process in terms of the spark location, weaves orientation, the composite type (unidirectional, multidirectional), and debris in the dielectric and tool wear, etc.

Once the discharge is completed, the heat travels to the inner parts of the workpiece and the surface temperature significantly drops due to the absence of the heat source. The heat is conducted to the neighbouring fibres, and the epoxy matrix’s temperature increases, preparing the next layer of material to be easily removed by the next spark.

The temperature distribution across the depth is very important because it indicates how deep the heat travels into the materials at certain times, allowing us to determine the heat-affected zones and the delamination depth.

## 4 Conclusion

Traditionally, the drilling of CFRP using electrical discharge machining has relied solely on a die-sink configuration. This study innovatively applies wire EDM for the first time to drill thick CFRP lay-ups, specifically unidirectional and multidirectional, with a thickness of 9.36 mm, without using assisted electrodes. The study confirmed the viability of WEDM for drilling CFRP, and its primary findings are summarized as follows:

- The multidirectional lay-up exhibited significantly higher MRR, up to 2.85 mm<sup>3</sup>/min, compared to a maximum of just 0.95 mm<sup>3</sup>/min for the unidirectional configuration under the same cutting conditions. The uniform fibre-matrix interaction irrespective of wire direction in the multidirectional composite promoted this faster and more consistent material removal.
- Increasing ignition currents up to 5 A enhanced material removal rates in both lay-ups. However, due to the composite's inherent low conductivity and heterogeneity, this led to various types of damage on machined surfaces such as delamination, uneven hole edges, frayed surface fibres, resin debris, and reduced circularity, especially notable in the unidirectional lay-up due to non-uniform wire-matrix interaction.
- The highest top DF of 1.4 was observed in the multidirectional lay-up at 5 A and 6 μs, whereas the unidirectional lay-up reached its peak bottom DF of 1.24 under identical cutting conditions. These opposing trends in top and bottom delamination factors across both lay-ups stem from CFRP's anisotropic nature, flushing effectiveness, and thermal gradients from top to bottom. Specifically, reducing the pulse-off time to 4 μs in multidirectional CFRP results in reduced delamination factors and improved circularity
- No parameters exhibited statistically significant effects on MRR, top DF, or bottom DF. However, the lay-up showed the highest PCR for MRR at 40.83%, followed by IAL at 29.46%. Regarding delamination, IAL had the highest PCR of 33% for the top DF and 27.01% for the bottom DF. The interactions between lay-ups and machining parameters revealed substantial PCR values: 26.82% for the top (B × lay-up) and 43.75% for the bottom (IAI × lay-up).
- The analytical solution reveals that a single discharge elevates the surface temperature above the sublimation point of CFRP, leading to the removal of approximately 45 μm from the matrix. This removal is attributed to the rapid heat conduction facilitated by the high conductivity of carbon fibres. These findings align well with experimental observations of thermal damage and delamination, with length typically falling within the range of 30–50 μm. The model also provides valuable insights into the dynamic changes in the temperature gradient over time.

In summary, the study reveals that WEDM demonstrates effectiveness in drilling CFRP composites, and multidirectional CFRP lay-ups exhibit superior hole quality and higher machining efficiency than unidirectional configurations.

**Author contribution** All authors contributed to the study conception and design. Material preparation, data collection, statistical analysis, and analytical modelling were performed by Aman Bajoria, Ahmad Alshaer, and Ramy Abdallah. The first draft of the manuscript was written by Aman Bajoria, and all authors commented on previous versions of the manuscript. All authors read and approved the final manuscript.

## Declarations

**Competing interests** The authors declare no competing interests.

**Open Access** This article is licensed under a Creative Commons Attribution 4.0 International License, which permits use, sharing, adaptation, distribution and reproduction in any medium or format, as long as you give appropriate credit to the original author(s) and the source, provide a link to the Creative Commons licence, and indicate if changes were made. The images or other third party material in this article are included in the article's Creative Commons licence, unless indicated otherwise in a credit line to the material. If material is not included in the article's Creative Commons licence and your intended use is not permitted by statutory regulation or exceeds the permitted use, you will need to obtain permission directly from the copyright holder. To view a copy of this licence, visit <http://creativecommons.org/licenses/by/4.0/>.

## References

1. Fekete J, Hall J (2017) Design of auto body: materials perspective. *Automot Steels* 1–18. <https://doi.org/10.1016/B978-0-08-100638-2.00001-8>
2. Mohee FM, Al-Mayah A, Plumtree A (2016) Anchors for CFRP plates: state-of-the-art review and future potential. *Compos B: Eng* 90:432–442. <https://doi.org/10.1016/j.compositesb.2016.01.011>
3. Li Z, Meng Z (2016) A review of the radio frequency non-destructive testing for carbon-fibre composites. *Meas Sci Rev* 2:68–76. <https://doi.org/10.1515/msr-2016-0010>
4. Akematsu Y, Kageyama K, Murayama H (2016) Basic characteristics of electrical discharge on CFRP by using thermal camera. *Procedia CIRP* 42:197–200. <https://doi.org/10.1016/j.procir.2016.02.270>
5. Qiu X, Li P, Niu Q, Chen A, Ouyang P, Li C, Ko TJ (2018) Influence of machining parameters and tool structure on cutting force and hole wall damage in drilling CFRP with stepped drills. *Int J Adv Manuf Technol* 1–9. <https://doi.org/10.1007/s00170-018-1981-2>
6. Zhang J, Lin G, Vaidya U, Wang H (2022) Past, present and future perspective of global carbon fibre composite developments and applications. *Compos B: Eng* 250:110463. <https://doi.org/10.1016/j.compositesb.2022.110463>
7. El-Hofy MH, Soo SL, Aspinwall DK, Sim WM, Pearson D, M'Saoubi R, Harden P (2017) Tool temperature in slotting of CFRP composites. *Procedia Manuf* 10:371–381. <https://doi.org/10.1016/j.promfg.2017.07.007>
8. Sheikh-Ahmad JY, Shinde SR (2016) Machinability of carbon/epoxy composites by electrical discharge machining. *Int J Mach*

- Mach Mater 18(1–2):3–17. <https://doi.org/10.1504/IJMMM.2016.075452>
9. Jia ZY, Chen C, Wang FJ, Zhang C, Wang Q (2020) Analytical model for delamination of CFRP during drilling of CFRP/metal stacks. *Int J Adv Manuf Technol* 106:5099–5109. <https://doi.org/10.1007/s00170-020-05029-y>
  10. Sun L, Gao H, Wang B, Bao Y, Wang M, Ma S (2020) Mechanism of reduction of damage during helical milling of titanium/CFRP/aluminium stacks. *Int J Adv Manuf Technol* 107(11–12):4741–4753. <https://doi.org/10.1007/s00170-020-05177-1>
  11. Geier N, Szalay T, Takács M (2019) Analysis of thrust force and characteristics of uncut fibres at non-conventional oriented drilling of unidirectional carbon fibre-reinforced plastic (UD-CFRP) composite laminates. *Int J Adv Manuf Technol* 100(9–12):3139–3154. <https://doi.org/10.1007/s00170-018-2895-8>
  12. Al-wandi S, Ding S, Mo J (2017) An approach to evaluate delamination factor when drilling carbon fiber-reinforced plastics using different drill geometries: experiment and finite element study. *Int J Adv Manuf Technol* 93(9–12):4043–4061. <https://doi.org/10.1007/s00170-017-0880-2>
  13. Wang H, Ning F, Hu Y, Li Y, Wang X, Cong W (2018) Edge trimming of carbon fiber-reinforced plastic composites using rotary ultrasonic machining: effects of tool orientations. *Int J Adv Manuf Technol* 98(5–8):1641–1653. <https://doi.org/10.1007/s00170-018-2355-5>
  14. Dhanawade A, Kumar S (2017) Experimental study of delamination and kerf geometry of carbon epoxy composite machined by abrasive water jet. *J Compos Mater* 51(24):3373–3390. <https://doi.org/10.1177/0021998316688950>
  15. Hu J, Zhu D (2018) Investigation of carbon fiber reinforced plastics machining using 355 nm picosecond pulsed laser. *Appl Compos Mater* 25(3):589–600. <https://doi.org/10.1007/s10443-017-9637-1>
  16. Habib S, Okada A (2016) Influence of electrical discharge machining parameters on cutting parameters of carbon fiber-reinforced plastic. *Mach Sci Technol* 20(1):99–114. <https://www.tandfonline.com/doi/pdf/10.1080/10910344.2015.1133914?> Accessed 20 Jun 2024
  17. Sheikh-Ahmad JY (2016) Hole quality and damage in drilling carbon-epoxy composites by electrical discharge machining. *Mater Manuf Process* 31(7):41–950. <https://www.tandfonline.com/doi/pdf/10.1080/10426914.2015.1048368?> Accessed 20 Jun 2024
  18. Wang T, Wu D (2023) A modified conductive network used to characterize the conductivity of carbon fibre reinforced polymers in eddy current testing. *Compos Struct* 314:116948. <https://doi.org/10.1016/j.compstruct.2023.116948>
  19. Lau W, Wang M, Lee W (1990) Electrical discharge machining of carbon fibre composite materials. *Int J Mach Tools Manuf* 30(2):297–308. <https://www.sciencedirect.com/science/article/pii/0890695590901389?via%3Dihub>. Accessed 20 Jun 2024
  20. Habib S, Okada A, Ichii S (2013) Effect of cutting direction on machining of carbon fibre reinforced plastic by electrical discharge machining process. *Int J Mach Mach Mater* 13(4):414–427. <https://doi.org/10.1504/IJMMM.2013.054272>
  21. Ichii S, Okada A, Okamoto Y, Uno Y (2011) Influence of carbon fiber direction on EDM characteristics of CFRP. *Int Conf Lead Edge Manuf 21st Century, LEM 1–4*. [https://doi.org/10.1299/jsmelem.2011.6\\_3247-1](https://doi.org/10.1299/jsmelem.2011.6_3247-1)
  22. Roldan-Jimenez L, Bañon F, Valerga AP, Fernandez-Vidal SR (2022) Design and analysis of CFRP drilling by electrical discharge machining. *Polym* 14(7):1340. <https://doi.org/10.3390/polym14071340>
  23. Pattanayak S, Sahoo AK, Sahoo SK (2022) CFRP composite drilling through electrical discharge machining using aluminum as fixture plate. *Proc Inst Mech Eng C* 236(10):5468–5483. <https://doi.org/10.1177/09544062211058675>
  24. Chen N, Kong L, Lei W, Qiu R (2023) Experimental study on EDM of CFRP based on graphene aqueous solution. *Mater Manuf Process* 38(9):1180–1189. <https://doi.org/10.1080/10426914.2023.2165674>
  25. Kumaran VU, Kliuev BR, Wegener K (2020) Influence of carbon-based fillers on EDM machinability of CFRP. *Procedia CIRP* 95:437–442. <https://doi.org/10.1016/j.procir.2020.03.153>
  26. Yue X, Yang X, Tian J, He Z, Fan Y (2018) Thermal, mechanical and chemical material removal mechanism of carbon fiber reinforced polymers in electrical discharge machining. *Int J Mach Tools Manuf* 133:4–17. <https://doi.org/10.1016/j.ijmactools.2018.05.004>
  27. Park S, Kim G, Lee W, Min B, Lee S, Kim T (2015) Microhole machining on precision CFRP components using electrical discharging machining. In: 20th Int Conf Compos Mater, Copenhagen, Denmark
  28. Kaushik N, Jha SK, Experimental ARS (2023) Investigation of micro EDM drilling in the CFRP using response surface methodology. *Front Mater* 10:1147882. <https://doi.org/10.3389/fmats.2023.1147882>
  29. Kumar R, Kumar A, Singh I (2018) Electric discharge drilling of micro holes in CFRP laminates. *J Mater Process Technol* 259:150–158. <https://doi.org/10.1016/j.jmatprotec.2018.04.031>
  30. Kumar R, Agrawal PK, Singh I (2018) Fabrication of micro holes in CFRP laminates using EDM. *J Manuf Process* 59–866. <https://doi.org/10.1016/j.jmapro.2018.01.011>
  31. Makudapathy C, Sundaram M (2020) High aspect ratio machining of carbon fiber reinforced plastics by electrical discharge machining process. *J Micro Nano-Manuf* 8:041005(1–5). <https://doi.org/10.1115/1.4049420>
  32. Dutta H, Debnath K, Sarma DK (2019) A study of material removal and surface characteristics in micro-electrical discharge machining of carbon fiber-reinforced plastics. *Polym Compos* 40(10):4033–4041. <https://doi.org/10.1002/pc.25264>
  33. Kumar P, Vivek J, Senniagir N, Nagarajan S, Chandrasekaran K (2022) A study of added sic powder in kerosene for the blind square hole machining of CFRP using electrical discharge machining. *SILICON* 14(4):1831–1849. <https://doi.org/10.1007/s12633-021-01243-9>
  34. Islam MM, Li CP, Won SJ, Ko TJ (2017) A deburring strategy in drilled hole of CFRP composites using EDM process. *J Alloys Compd* 703:477–485. <https://doi.org/10.1016/j.jallcom.2017.02.001>
  35. Lau W, Lee W (1991) A comparison between EDM wire-cut and laser cutting of carbon fibre composite materials. *Mater Manuf Process* 6(2):331–342. <https://www.tandfonline.com/doi/abs/10.1080/10426919108934760>. Accessed 20 Jun 2024
  36. Abdallah R, Soo SL, Hood R (2021) The influence of cut direction and process parameters in wire electrical discharge machining of carbon fibre-reinforced plastic composites. *Int J Adv Manuf Technol* 113:1699–1716. <https://doi.org/10.1007/s00170-021-06641-2>
  37. Abdallah R, Hood R, Soo SL (2022) The machinability characteristics of multidirectional CFRP composites using high-performance wire EDM electrodes. *J Compos Sci* 6(6):159. <https://doi.org/10.3390/jcs6060159>
  38. Wu C, Cao S, Zhao YJ, Qi X, Liu G, Guo J, Li HN (2020) Preheating assisted wire EDM of semi-conductive CFRPs: principle and Anisotropy. *J Mater Process Technol* 288:116915. <https://doi.org/10.1016/j.jmatprotec.2020.116915>
  39. Dutta H, Debnath K, Sarma DK (2021) Investigation on cutting of thin carbon fiber-reinforced polymer composite plate using sandwich electrode-assisted wire electrical-discharge machining. *Proc Inst Mech Eng E* 235(5):1628–1638. <https://doi.org/10.1177/09544089211013318>
  40. Anbalagan A, Venugopal A, Anthony XM, Pazhani A, Batako A (2023) Novel machining configuration of carbon fibre reinforced polymer (CFRP) using wire electric discharge machining

- (WEDM). *Int Conf Intell Syst Prod Eng Maint*, Springer: 16–24. [https://doi.org/10.1007/978-3-031-44282-7\\_2](https://doi.org/10.1007/978-3-031-44282-7_2)
41. AbouHawa M, Eissa A (2024) Corner cutting accuracy for thin-walled CFRPC parts using HS-WEDM. *Discov Appl Sci* 6(3):130. <https://doi.org/10.1007/s42452-024-05766-9>
  42. Chen WC (1997) Some experimental investigations in the drilling of carbon fiber-reinforced plastic (CFRP) composite laminates. *Int J Mach Tools Manuf* 37(8):1097–1108. [https://doi.org/10.1016/S0890-6955\(96\)00095-8](https://doi.org/10.1016/S0890-6955(96)00095-8)
  43. Alshaer AW, Rogers BD, Li L (2017) Smoothed particle hydrodynamics (SPH) modelling of transient heat transfer in pulsed laser ablation of Al and associated free-surface problems. *Comput Mater Sci* 127:161–179. <https://doi.org/10.1016/j.commatsci.2016.09.004>
  44. Assarzadeh S, Ghoreishi M (2017) Electro-thermal-based finite element simulation and experimental validation of material removal in static gap single-spark die-sinking electro-discharge machining process. *Proc Inst Mech Eng B* 231(1):28–47. <https://doi.org/10.1177/0954405415572>
  45. Murali MS, Yeo SH (2005) Process simulation and residual stress estimation of micro-electrodischarge machining using finite element method. *Jpn J Appl Phys* 44(7R):5254. <https://doi.org/10.1143/JJAP.44.5254>
  46. Minus M, Kumar S (2005) The processing, properties, and structure of carbon fibers. *JOM* 57(2):52–58. <https://link.springer.com/article/10.1007/s11837-005-0217-8>. Accessed 20 Jun 2024)
  47. Elements A. American Elements. Carbon fibre product datasheet C-E-01-FIB. <https://www.americanelements.com/carbon-fiber-7440-44-0>. Accessed 20 Jun 2024
  48. Resin (epoxy) melting point boiling point density CAS chemical properties-24969-06-0 CAS MSDS. [https://www.chemicalbook.com/ChemicalProductProperty\\_US\\_CB2701716.aspx](https://www.chemicalbook.com/ChemicalProductProperty_US_CB2701716.aspx). Accessed 20 Jun 2024
  49. Wang H, Habib S, Okada A, Uno U (2010) EDM characteristics of carbon fiber reinforced plastic. *Proc 16th Int Symp Electromach* 65:68
  50. Abdallah R, Soo SL, Hood R (2018) A feasibility study on wire electrical discharge machining of carbon fibre reinforced plastic composites. *Procedia CIRP* 77:195–198. <https://doi.org/10.1016/j.procir.2018.08.284>
  51. Ablyaz TR, Shlykov ES, Muratov KR, Sidhu SS (2021) Analysis of wire-cut electro discharge machining of polymer composite materials. *Micromachines* 12(5):571(1:14). <https://doi.org/10.3390/mi12050571>

**Publisher's Note** Springer Nature remains neutral with regard to jurisdictional claims in published maps and institutional affiliations.